Development of a Mission-Tailored Tail-Sitter MAV

Luiz F. T. Fernandez, Murat Bronz, Nathalie Bartoli, Thierry Lefebvre

Unmanned Systems, Vol. 0, No. 0 (2013) 1–15

Development of a Mission-Tailored Tail-Sitter MAV

Luiz F. T. Fernandez[a,b], Murat Bronz[b], Nathalie Bartoli[b], Thierry Lefebvre[b]

[a] *ONERA/DTIS, Université de Toulouse, Toulouse, France*
E-mail:luiz.tiberio@onera.fr

[b] *ENAC, Université de Toulouse, F-31400 Toulouse, France*

Vertical takeoff and landing (VTOL) vehicles are among the most versatile UAVs, appropriate for various missions. Given that there are still open challenges regarding the VTOL design, this paper presents the full development and test cycle of a tail-sitter. IMAV 2022 competition rules were used to define the mission. A multidisciplinary design and optimization strategy was defined with the goal of maximizing competition score considering design, manufacturing, and competition constraints. The resulting vehicle was designed to fly at 18 m/s while carrying 200 g of payload with a total weight of approximately 720 g. It flew for roughly 13 minutes at IMAV2022, helping its team to achieve 1st place at the "Package delivery challenge". Further flight tests revealed the ultimate endurance performance as 18 minutes.

Keywords: Multidisciplinary Design and Optimization, Hybrid MAV Design, Transitioning MAV Design

1. Introduction

Unmanned aerial vehicles (UAVs) have been the object of study of several different research areas in the last decades. One can attribute this fact to two main reasons. From one side, such kind of vehicle can potentially be used for different missions, both civil and military. On the other hand, the technology poses a big variety of challenges to the aerial robotics community, which has primarily emerged from aerospace and robotics engineering fields. This community leverages from the fact that these vehicles can be designed and built with minimal cost, making it very attractive for real world testing and deployment. On the application side, there has been studies to use drones for fire fighting,[1,2] for searching marine debris,[3] and even for covid mitigation.[4] Along with several studies regarding perception,[5,6] control is arguably one of the most studied fields within the UAV community[7–9] just to name a few. As for the design aspect of UAVs and specially micro aerial vehicles (MAVs), fewer studies have been published. Wang et al.[10] presented a preliminary design methodology for small tail-sitters that considers weight and power models. Holsten et al.[11] presented the design strategy and wind tunnel test results for a multipurpose tilt-wing platform. Vogeltanz[12] presented the design and analysis of the mini-UAV tail-sitter named "V-TS", including 2D and 3D high fidelity aerodynamic analysis and flight dynamics modeling. A very extensive review on design and flight control techniques is presented by Ducard and Allenspach.[13]

Fig. 1: Sequential imagery of vertical take-off and transition in a test flight and vehicle ready for IMAV competition.

As we present the full development cycle of the MAV shown in Figure 1, the objectives of the paper are twofold:

- Throughout such process, we show how MDO techniques can be used to design mission adapted MAVs, while explaining how the algorithm was implemented and employed. In this context, MAV competitions are interesting as they pose well-defined missions, suitable for testing and comparing design strategies.
- By leveraging from the fact that MAVs are easier to manufacture and test when compared with commercial aircraft, this paper is also intended to show how the MDO process evolved, presenting its initial formulation, followed by experimental vali-

dation through wind tunnel and flight tests, and posterior refinement with final validation on the competition and further endurance tests.

In order to comply with this second objective, we present this paper in an unusual chronological fashion. This choice was made to facilitate the understanding of some design decisions and specially to show the rationale behind the entire MDO development. We start the paper with an overview about the IMAV 2022 competition rules and score calculation. Then our design philosophy and initial optimization strategy are detailed, and the manufacturing techniques are shown. The gathered knowledge from initial flight tests and wind tunnel test campaigns is then used to refine the MDO process and obtain the final vehicle, named *Falcon*. The competition results and complementary endurance tests are discussed, and conclusions and perspectives are presented.

2. Competition Rules and score analysis

The IMAV 2022 "Delivery far and fast" was a part of the "Package delivery competition" and was held in the Netherlands. The overall mission objective was to design and operate an MAV capable of carrying a specific amount of payload in a designated outdoor flight field. The score was defined as:

$$score = \frac{N_{laps}(D+1)AP}{W_{vehicle}/W_{max}} \tag{1}$$

Table 1 describes each component of Eq. (1).

Table 1: Score factors

Parameter	Definition
N_{laps}	number of laps
D	1 if landed with payload and 0 otherwise
A	Autonomy level
P	Payload point factor
$W_{vehicle}$	Vehicle weight
W_{max}	Maximum allowed weight of 5kg

Given that P1 and P2 are obstacles located at $500m$ from each other, a lap can be defined in the following order: visit the line orthogonal to the line P1P2, pass through P1, visit the line orthogonal to the line P1P2 again, and pass through P2. Figure 2 shows a representation of the mission and two compliant trajectories (black and red lines).

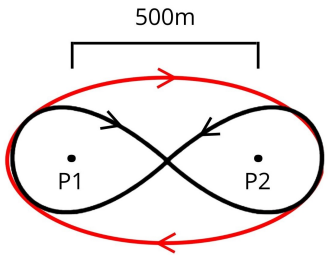

Fig. 2: Schematics of competition track and trajectories

The autonomy level (A) can assume the values: 1 (remote piloted UAV through video link), 2 (autonomous flight control), and 5 (autonomous mission control). The point factor (P) is defined as a function of the payload, as shown in Table 2.

Table 2: Payload and Points factor

Payload package mass $[g]$	P (Points factor)
100	1
200	2
500	3
1000	4

Throughout this paper, we will assume that the mission is fully autonomous ($A = 5$), and no additional constraints for landing would be used to handle the parameter "D". The overall mission time was constrained to 30 minutes, including not only the full flight, but also the time expended to put the vehicle in the flight arena and turn on the electronics. So, a maximum flight time of 23 minutes was assumed.

From Eq. (1), we can observe that the mission score is mainly driven by the number of laps (N_{laps}) and vehicle weight ($W_{vehicle}$). As the number of laps is mainly a function of flight velocity, increasing this factor might imply in greater propulsion, battery and structural weight, which in turn is reversely proportional to the score. Thus, there is an implicit trade-off in the score equation with respect to flight speed and vehicle weight. Such particularity makes the selection of design point more complicated when using traditional design techniques, as too much emphasis could be given to only one aspect of mission score. We used a Multidisciplinary Design Optimization (MDO) approach that allowed us not only to better explore the design space and the trade-off, but specially to find the optimal design with respect to the score.

3. Design Philosophy

The initial hypothesis was that a flying wing tail-sitter with four motors and no aerodynamic control surfaces was

[a] https://www.foxtechfpv.com/

[b] https://transition-robotics.com/pages/projects

the most suitable configuration for this mission. The usage of four motors allows for vectorized thrust based control, which in turn removes the necessity of control surfaces and additional servos, reducing complexity in the manufacturing process. Such choice also enables more precise landing than other tail-sitter configurations that relies on flaps for pitch authority, as such vehicles can present control inefficiencies at low speeds. Figure 3 shows two MAVs used as baseline for our design process, the H-wing by Foxtech[a], and the QuadShot[b] by Transition Robotics. Considering the time limitation between the publication of the competition rules and the competition itself, we decided not to search for new motors on the market, but to use the ones already available at ENAC drone lab. This decision reduced the design freedom, but considering time and geographic constraints, buying new motors would reduce the amount of flight experiments with the whole vehicle and control system, which has proven to be of paramount importance, as explained in the following sections. So, the smallest motor available was selected, the `F1507` by `T motor`[c]. The propeller selection is discussed in Section 4.6.

(a) FoxTech H-wing

(b) Transition Robotics QuadShot

Fig. 3: Baseline designs

The employed MDO approach was formulated to maximize the competition score by varying wing planform, angle of attack, and battery mass. Figure 4 shows the **E**xtended **D**esign **S**tructure **M**atrix, as proposed by Lambe and Martins,[14] created using WhatsOpt,[15] a web application for MDO developed at ONERA. The optimization process employs the Multi Disciplinary Feasible architecture (MDF),[16] which consists of a Multidisciplinary Analysis Module (MDA) and the mission score calculation. The MDA is a system of equations of three different disciplines: aerodynamics, mission analysis, and weights, which are described in the following sections. It is a non-linear system because of how the inputs and outputs of each discipline are correlated. In this case, the cruise speed V_{cruise} is the output of the mission module, which uses the output of the aerodynamic module, lift and drag coefficients, to estimate the range. On the other hand, the aerodynamic module requires the V_{cruise} to calculate its outputs, lift and drag coefficients. To ensure that this non-linear system is always feasible, the MDF architecture uses a non-linear solver, which is called by the optimizer for every optimization iteration. As opposed to classical design techniques, where a variable (e.g. C_L) has to be fixed, limiting the design space and possibly leading to suboptimal solutions, this MDO approach allows for more space exploration while still ensuring feasibility. As the design variables, shown in the upmost left block in Figure 4, change, the inputs (upper right gray boxes) and the outputs (lower left gray boxes) for every discipline change as well.

3.1. *Aerodynamic analysis*

OpenAeroStruct[17] (OAS), a lightweight tool capable of performing aerostructural optimization, was used for the wing aerodynamic analysis. It uses a vortex lattice method (VLM) to calculate aerodynamic coefficients. The MH45 airfoil was selected for the first iteration of the analysis. Table 3 shows that the payload dimensions, stipulated by the competition, are representative when compared to general MAV dimensions, so its drag can not be disregarded.

Table 3: Payload dimensions

Payload mass $[g]$	length × width × height $[mm]$
100	$100 \times 60 \times 40$
200	$100 \times 80 \times 60$
500	$150 \times 100 \times 70$
1000	$145 \times 130 \times 110$

Even if a greater payload tends to increase the score when considering the points factor (P), this choice would directly lead to greater weights, both structural and battery, and drag. The payload, which is a rectangular body, drag coefficient ($C_{D_{Payload}}$) was fixed to 1.2 according to Carvill.[18] Summarizing, the aerodynamic module calculates the total lift and drag coefficients for a given wing geometry, payload mass, and flight velocity.

3.2. *Mission analysis and sizing*

The mission module calculates flight speed, range, endurance, and number of laps for a given set of aerodynamic coefficients, wing area, MAV total mass, and battery mass. The cruise velocity (V_{cr}) is calculated to reinforce that lift is equal to weight in non-accelerated flight as:

$$V_{cr} = \sqrt{\frac{m_{mav} g}{0.5 \rho S C_L}} \tag{2}$$

where m_{mav} is the vehicle mass, g the gravity acceleration, ρ the air density, S the wing reference area, and C_L the lift coefficient in cruise condition. The flight range (R) can be obtained for a given battery mass (m_{bat}) and vehicle mass as:

$$R = \frac{m_{bat}}{m_{mav} g} B_{SE} \eta \frac{C_L}{C_D} \tag{3}$$

[c] `https://store.tmotor.com/goods-923-F1507+KV2700.html`

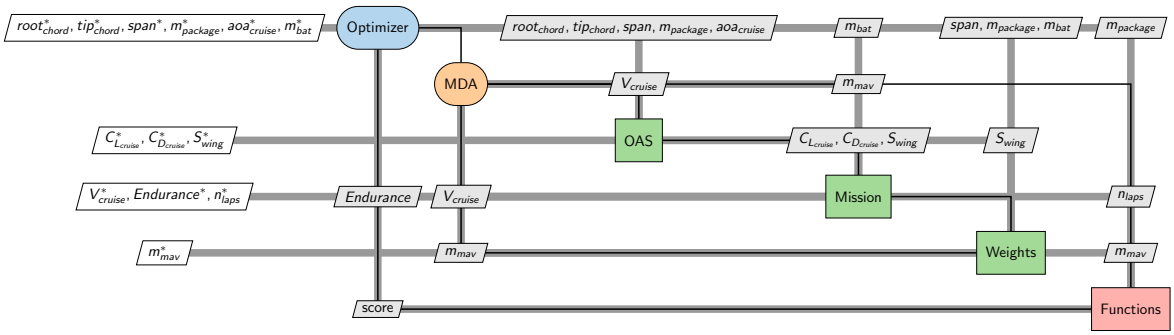

Fig. 4: Extended design structure matrix of the tail-sitter process

where C_D is the drag coefficient in cruise, the battery specific energy (B_{SE}) was assumed to be 133 $\frac{Wh}{kg}$ and overall propulsive system efficiency η was assumed to be 0.32. Flight endurance (E) is then:

$$E = \frac{R}{V_{cr}}. \tag{4}$$

In order to obtain the number of laps, the lap distance was decomposed into two parts of straight 500 m level flight, and two turns. The turn radius is calculated as:

$$T_R = \frac{V_{cr}^2}{g\sqrt{n^2-1}} \tag{5}$$

where the load factor (n) was fixed in 1.5, which corresponds to an approximately 50° bank. The number of laps was then obtained as the integer part of the ratio between flight range and lap distance:

$$N_{laps} = \lfloor \frac{R}{500 + 500 + 2\pi T_R} \rfloor \tag{6}$$

3.3. *Weights module*

The MAV total weight is obtained as a sum of electronics, battery, wing spar, and structural weight. Table 4 shows the weight breakdown of fixed components.

Table 4: Fixed weight breakdown.

Component	Mass [g]
Autopilot	12.0
Xbee module	5.2
Speed controller	20.7
RC receiver	7.7
Motor (each)	17.0
Motor arm (each)	35.0
GPS module	50.0
Cables	30.0

Considering previous experience with 3D printed structures from[19] we chose to use this manufacturing technique for the wings. Two carbon tubular spars with 50% span length were used. Previous experience also shows that the usage of two spars instead of one provides better rigidity, restricts the rotation motion and eases component assembly. Also, the reduction in the spar length does not compromise the wingtip structural integrity and allows for weight reduction. In order to estimate the weight of the structure, we used high and low quality existing printed pieces to obtain an average of the surface weight as a function of its area. The obtained results are shown in Table 5.

Table 5: 3D printed structure weight as function of its area

Structural rigidity	density of area [g/m^2]
High	2485
Low	941
Average	1713

The wing spar weight was calculated considering a 5mm carbon tube.

3.4. *MDO implementation*

The MDO loop was implemented using OpenMDAO,[20] an open-source framework for efficient multidisciplinary optimization, and all the models were implemented in Python. The non-linear Gauss-Seidel method was selected for solving the MDA, and we used IPOPT (Interior Point OPTimizer) from PyOptSparse[21] as the optimizer. Table 6 shows the design variables, objective function, and constraint. For the optimization, the mission score is calculated as:

$$\text{Score} = N_{laps}\frac{P}{m_{mav}g} \tag{7}$$

Table 6: MDO problem formulation.

	Function/Variable	Lower	Upper
Maximize	Score		
With respect to	Root chord	0.09 m	0.4 m
	Tip chord	0.05 m	0.4 m
	Span	0.3 m	1.0 m
	Cruise α	$-10°$	$10°$
	Battery mass	0.01 kg	1.00 kg
Subject to	Endurance $\leq$ 23 min		

3.5. *Design analysis*

We started our analysis by evaluating how the competition score was affected by the different allowed payloads. For that, the MDO was executed four times, each of them for a fixed payload value, shown in Table 3. Figure 5 shows the characteristics of the obtained vehicles. It can be noted that choosing the smaller payload possible (100 g) would lead to a non-competitive score, while the best values were found for the higher payloads.

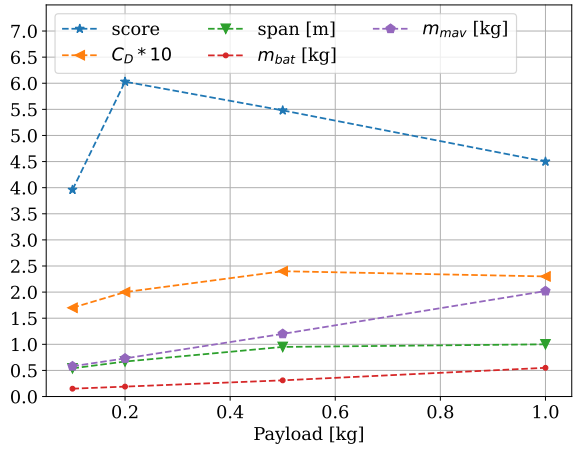

Fig. 5: Maximized score, wing span and total drag for the allowed payloads.

As it would be expected, the increase in payload mass also leads to bigger wing areas, which in turn increases the drag in cruise. The biggest payload designs are penalized by the drag generated by the bigger fuselage and wing. Figure 5 also shows that the observed difference in drag generates a significant difference in terms of battery and total weight.

This analysis showed that using 200 g of payload mass for the first design iteration would be beneficial. Table 7 shows the characteristics of the optimized MAV design.

Table 7: Optimal MAV characteristics

Design variables	Value
Root chord	0.09 m
Tip chord	0.05 m
Wing span	0.66 m
Cruise α	8.73°
Battery mass	0.19 kg
Coupling variables	**Value**
Wing area	0.0467 m^2
Cruise speed	17.7 m/s
Cruise C_L	0.91
Cruise C_D	0.20
Flight time	23 min
Number of laps	21
MAV mass	0.74 kg

The optimizer drove both root and tip chords to the lower limits, leading to a small wing area design. Throughout the flight test campaign, this has proved to be a problem, caused by the overestimation of the lift generation, as discussed is Section 4.9.

4. Practical implementation and flight tests

In the following sections, we explain how the vehicle was built and prepared for flight. We also present the iterative flight test procedure, where the complexity of the mission was increased according to the outcome of each test.

4.1. *Manufacturing*

One of the main objectives of this work was to showcase the iterative refining of the MDO process for IMAV 2022's mission profile. Therefore, the agile manufacturing technique using 3D printing proposed in Bronz et al.[19] was chosen. Such strategy allows for rapid manufacturing of different parts, which in turn enables faster design iterations.

4.2. *Fuselage considerations*

In order to reduce manufacturing complexity and enable efficient competition-time repairs, we chose not to cover the center body, which includes the electronics, battery, and payload, with an "aerodynamic fuselage". The impact on flight range of adding this coverage and thus reducing drag and increasing weight was not analyzed because of this design decision. This choice also allowed the usage of the payload as a landing gear, removing the need for a dedicated structure for such task. Figure 6 shows the first prototype, ready to fly, with the 200 g package attached. The wing chord at the junction has been reduced with the objective of creating less interference (with fuselage) drag.

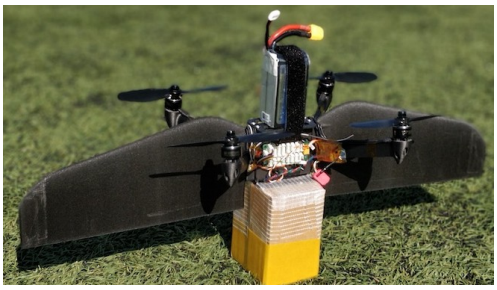

Fig. 6: First prototype.

4.3. *Flight control system*

We used Paparazzi[d] system,[22] which allows for the automation of flight tasks up to complete autonomous flight for a designated route. The already implemented INDI control law, successfully applied to a tail-sitter in[9] was employed. The gains were estimated based on previous experience and then refined after flight experiments. For the competition, the flight trajectory was defined through Paparazzi's flight plan, and all the flight phases were fulfilled autonomously, including safety measures such as low-battery and GPS-lost mitigation maneuvers.

4.4. *Hover tests*

The first hover test was conducted using only the main body of the vehicle inside ENAC's flight arena, as shown in Figure 7, while waiting for the manufacturing of the wing pairs. The gathered data were used to fine-tune the efficiency matrix of the INDI[9] controller for hover phase and proved that the vehicle was capable of stable hover with the designated payload. The wings were then assembled for the second hover test.

Fig. 7: Indoor hover test.

[d] https://wiki.paparazziuav.org/wiki/Main_Page

4.5. *Outdoor flight tests*

After successfully performing the hover tests, the vehicle was tested in an outdoor flight field. Throughout the first day of tests, six successful non-autonomous flights were performed, with increasing level of difficulty starting from simple hover to full flights with takeoff, cruise, and landing. Figure 8 shows the trajectory of the third flight, whose data will be shown from now on.

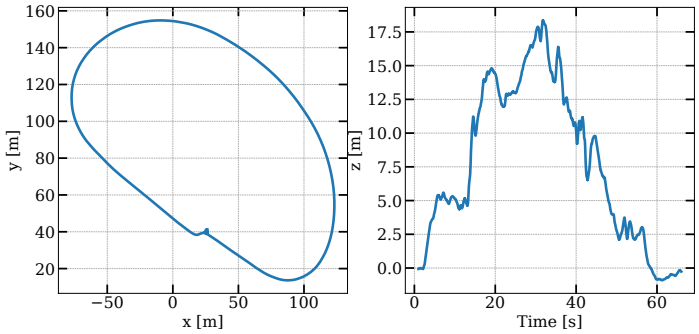

Fig. 8: Experimental flight trajectory in XY plane and altitude.

After this approximately one minute flight, the motors were overheated, indicating that an overload could be occurring. By analyzing Figure 9, that shows power consumption throughout the flight, it is indeed possible to note that even during cruise the motors were heavily loaded, and no significant difference was observed between hover and cruise, which should not be the case for a winged vehicle.

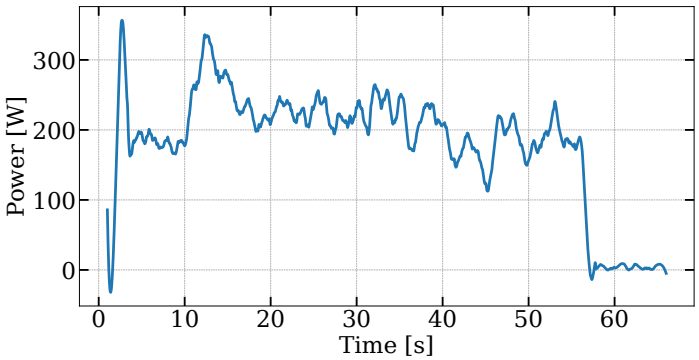

Fig. 9: Experimental flight power consumption.

With such high values of power, the vehicle would not be able to perform the proposed 23-minute mission. So it became necessary to investigate the source of such power consumption, with two main candidates:

- The set motors-propellers could be inadequate in terms of allowing for high range cruise and control authority. The only possibly suitable propellers available at that moment were the `GS 5x4.5`, but smaller diameters could increase cruise efficiency.
- The predicted drag polar could be overly optimistic for both lift and drag.

4.6. *Propulsion system testing and autonomous flights*

In order to compare different sizes of propellers and its impact on the performance, a new batch of outdoor tests was prepared and executed. We performed two fully autonomous flights, with the same trajectory and set points of 18 m/s and 30 m for cruise velocity and altitude, respectively. The only difference between flight 2 and flight 3 were the propellers, the already discussed `GS 5x4.5` (flight 2) and the smaller `GS 4x4.5` (flight 3) were used. The outcome in terms of trajectory was quite similar, as presented in Figure 10, which allows for a fair comparison between propellers.

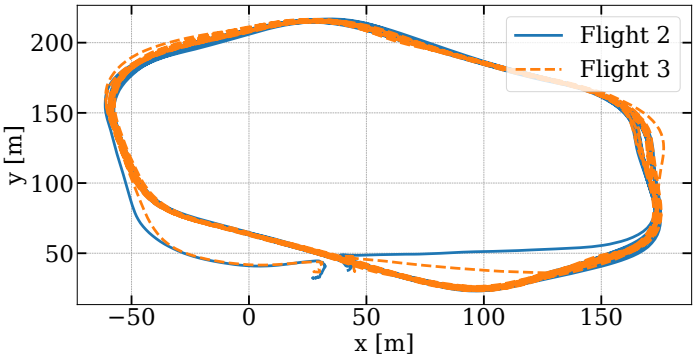

Fig. 10: Autonomous flight 2 and 3 trajectories in XY plane.

Figure 11 shows that flight 3, with the smaller propeller, shows indeed a slightly smaller current and presents a higher voltage at the end of the flight. However, such improvement would still not make desired flight time possible as the power demand was still high, as shown in Figure 12.

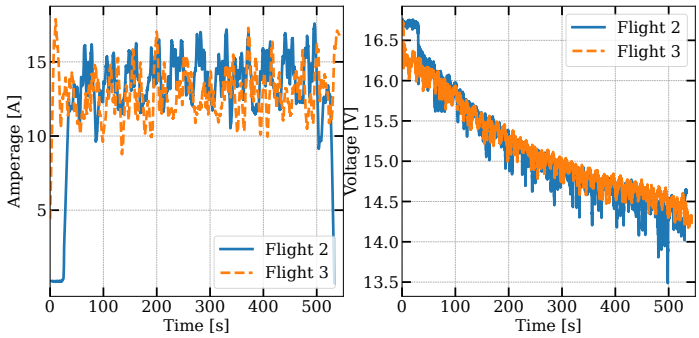

Fig. 11: Autonomous flight 2 and 3 current and voltage.

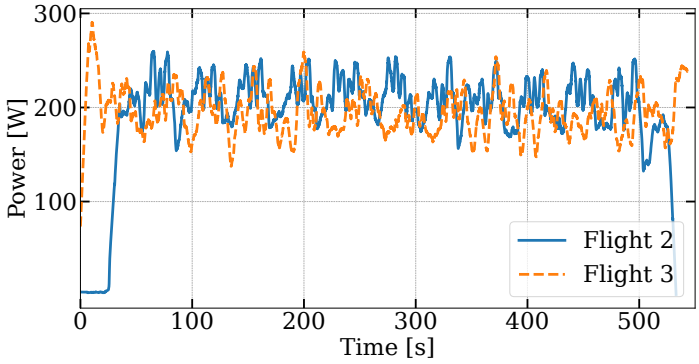

Fig. 12: Autonomous flight 2 and 3 power consumption.

As a result, the autonomous flight capability and its ability to reproduce commanded trajectories was validated, and the hypothesis that a bigger propeller was causing an increase in the energy consumption was confirmed, even though the influence was small. Nevertheless, we opted for including propeller analysis in the second iteration of the MDO, as discussed in Section 5.1.

4.7. *Wind Tunnel setup*

In order to validate both lift and drag predictions, the vehicle was tested in a wind tunnel. The experiments were performed inside ENAC's (French Civil Aviation University) flight arena in Toulouse, France. The wind tunnel, designed by WindShape[e], has a 1.5 m by 0.75 m open test section and is used both for research and educational purposes. Forces and moments were measured with a six-axis ATI Mini-40 sensor[f] calibrated with SI-40-2, with maximum force range of 40 N for F_{xy}, 120 N for F_z and 1/100 N resolution for xy and 1/50 N resolution for z. The 1/100 N resolution represents roughly 0.62% of the final vehicle theoretical drag, and the 1/50 N is about 0.28% of the final vehicle theoretical lift. The moment range is 2 Nm for M_{xyz} with a

[e] `https://windshape.com/technology/`

[f] `https://www.ati-ia.com/products/ft/ft_models.aspx?id=mini40`

$1/400\,Nm$ resolution. The vehicle was tested in a single representative velocity and for four equally spaced angles of attack between 0° and 22.5°. Figure 13 shows the vehicle in front of the test section.

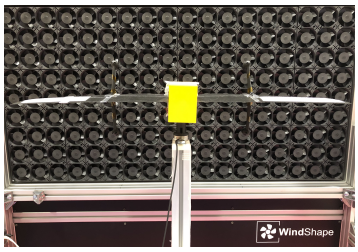

Fig. 13: Vehicle attached to the force and moment balance in front of WindShape.

4.8. *Drag evaluation*

Figure 14 shows an isometric and a side view of the concept with its components: wings, mounting motors arms with motors and propellers, payload, and the central piece that contains the electronics, pitot tube, and battery, from now on addressed as core.

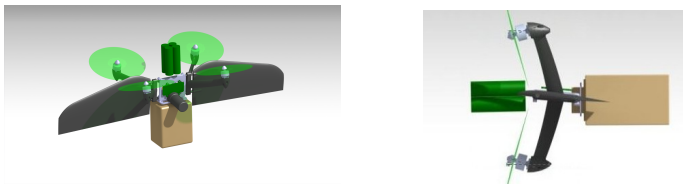

Fig. 14: Vehicle concept

Figure 15 shows the schematics of how the vehicle could be "dismounted" in order to identify the drag contribution of each drag source. The wing drag was obtained by subtracting the result of the wingless configuration ② from the full vehicle configuration ①. Similarly, the mounting arms drag was obtained by subtracting the result of the configuration without arms ③ from the full vehicle configuration ①. As the core is also used to fix the payload, it was not possible to isolate the effects of both components during the tests. So, the vehicle was tested without wings and without arms ④ to obtain the contribution of both components together and, to isolate the core, the vehicle was also tested without the payload configuration ⑤. The result of this test is shown in Figure 16.

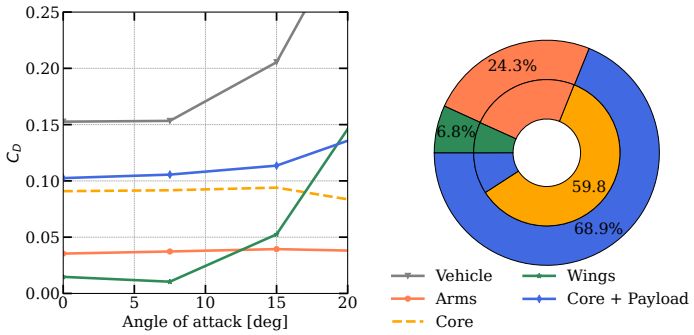

Fig. 16: Drag with respect to α and drag contributions at $\alpha = 7.5°$. The isolated core drag contribution is shown as a dashed line, and is already taken into account within the Core + Payload term for the drag breakdown

At low angles of attack, the Core + Payload term had the higher contribution in terms of drag generation. This behavior was expected once such parts were not aerodynamically optimized, but designed to be functional and to comply with operational (electronics and battery placement) and competition (fixed payload dimensions) constraints. Such outcome can be ameliorated with a further aerodynamic refinement. The mounting arms had the second higher drag contribution, almost constant with respect to the angle of attack, which can mainly be attributed to the fact that they are mainly "bluff bodies".

With this test, we observed that the drag was not underestimated at the analyzed angles. Therefore, it was not directly causing the high energy consumption problem. Nevertheless, the outcome of the test was used to refine the second version of the aerodynamic module of the MDO, as discussed in Section 5.2.

The test showed that, even tough the Core + Payload could not be changed because of the already mentioned constraints, the mounting arms had a significant contribution to the drag of the vehicle. Hence, we decided to evaluate a different configuration for this component, in order to reduce such behavior. Another vehicle was printed with the arms in "H" configuration, as shown in Figure 17.

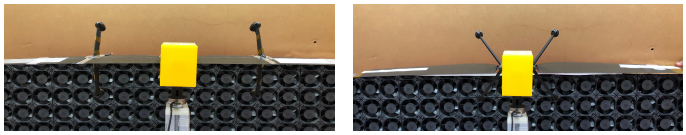

(a) Mounting arms in "H". (b) Mounting arms in "X".

Fig. 17: Test setup for arm configuration study. Half of the WindShape test section was covered to ease the visualization.

But little difference was observed in terms of drag. The "X" configuration arms led to slightly higher C_L for small angles of attack, as shown in Figure 18. Initially, we chose to maintain the "X" geometry mainly because of its sim-

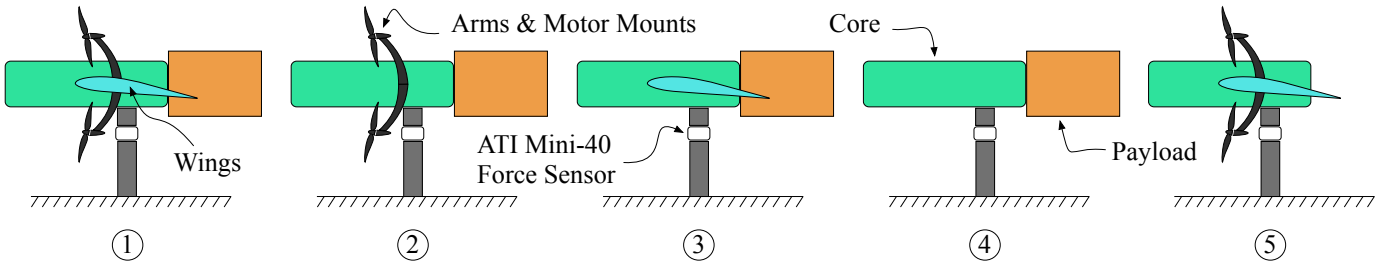

Fig. 15: Schematics of how the vehicle can be dismounted in order to isolate the drag contribution of each component.

plicity and light weight, but after flight tests we changed to "H" in order to increase the control authority.

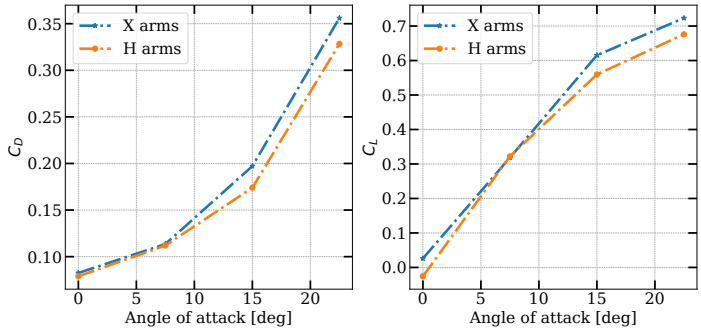

Fig. 18: Comparison of arm configuration.

4.9. *Lift evaluation*

By analyzing Figure 18, it is also possible to observe that the predicted C_L of 0.91 for an angle of attack of about 9°, shown in Table 7 was unfeasible. The actual value was less than half of the predicted value. The consequence of that can be seen in Figure 19, showing that pitch angle for both flight 2 and flight 3 was higher than 20° during the whole cruise flight, a flight regime that can be considered to be stalled, even if the real angle of attack is not known. As the wing lift was overestimated, the autopilot had to increase the pitch angle to ensure that the required force to compensate the weight was generated, but at such condition, only the motors were generating lifting force, while the stalled wings were mostly generating drag, penalizing flight efficiency.

[g] `https://github.com/byuflowlab/CCBlade.jl`

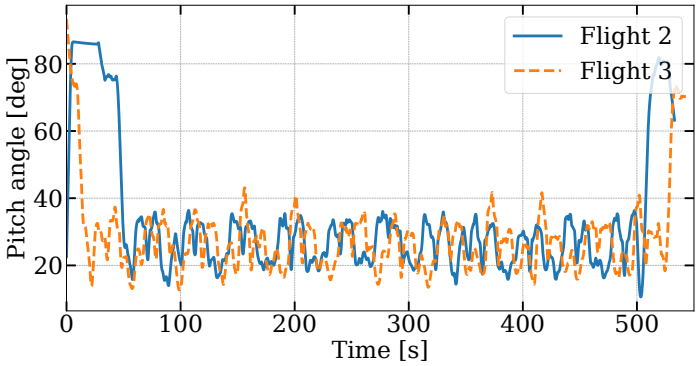

Fig. 19: Pitch angle for flights 2 and 3.

This is believed to have caused the lack of performance observed during the initial flights. The lack of lift was most likely generated by non-considered interference effects and 3D printing inaccuracies, while the process was still being refined. In order to handle that for the second iteration of the MDO, the lift output from OpenAerostruct was tuned to match the observed data, as detailed in Section 5.2.

5. MDO process refinement

The results obtained in the first batch of flight tests have shown that the initial MDO formulation was possibly over-simplified. The assumption made in Eq. (2) was that, in cruise, lift is equal to weight, and that the required thrust would be available throughout the entire flight. The outcome of the wind tunnel test has shown that the lift predicted with OpenAeroStruct was too optimistic, considering the manufacturing technology. This led to a small wing area, incapable of maintaining sustained level flight at low angles of attack, and culminating in poor flight performance. In order to refine our methodology and mitigate these effects, we have added a new discipline, new constraints for hover flight and turning maneuver and refined both the aerodynamic and weights modules.

5.1. *Propulsion refinement*

In order to obtain thrust (T) in both hover and cruise flight conditions, we employed CCBlade[g], a blade element momentum method formulation that is specially suited for gradient based optimization presented by Ning.[23] As CCBlade is implemented in Julia, we developed a wrapper to call it from our Python environment. With CCBlade, the thrust generated is calculated as a function of airspeed, propeller geometry and rpm. We employed Xfoil[24] to account for the propeller airfoil (approximated) polar in the optimization loop. In[25] we tested a UAV propeller in different advance ratios at ENAC's wind tunnel and compared the outcome of this test with several different analytical methodologies capable of calculating propeller performance at incidence. Figure 20 shows an example of the obtained results and that CCBlade is capable of accurately calculating propeller thrust. For further data, the reader is referred to.[25]

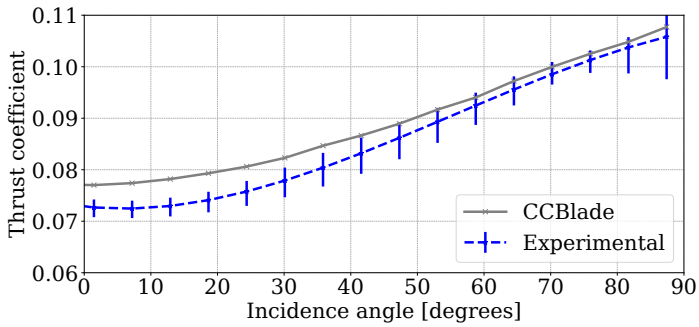

Fig. 20: Wind tunnel and CCBlade comparison for airspeed $= 6m/s$ and $\omega = 800rad/s$. The error bars were obtained considering the 7 different runs in which the experiment was conducted

In order to account for the hover capability, a new constraint was implemented:

$$a_{hover} = \frac{0.9T_0 - m_{mav}g}{m} \geq 0 \tag{8}$$

The acceleration in hover (a_{hover}), calculated as the difference between the static thrust (T_0) generated by the four propellers and MAV weight ($m_{mav}g$) was constrained to be greater than 0, in order to ensure hover capability. A safety margin of 10% was added to account for eventually necessary attitude corrections. Similarly, a constraint to ensure that in the forward flight axis there would be enough thrust to generate positive or zero acceleration (a_{turn}), was added:

$$a_{turn} = \frac{0.75T_{V_{turn}} - D}{m} \geq 0 \quad \text{at} \quad V_{turn} \tag{9}$$

where both lift ($C_{L_{turn}}$) and drag ($C_{D_{turn}}$) were also obtained using OpenAeroStruct. Thrust ($T_{V_{turn}}$) was then assumed as the sum of the thrust from all motors, calculated at turn velocity (V_{turn}), operating with a safety margin of 15%. V_{turn} was calculated as

$$V_{turn} = \sqrt{\frac{m_{mav}gn}{0.5\rho S C_{L_{turn}}}} \tag{10}$$

where the load factor n accounts for the decrease in lift generated by the bank angle. Considering this more detailed problem formulation, we were also able to refine range and endurance calculation. The turning radius from Eq. (5) could then be calculated as a function of V_{turn} :

$$T_R = \frac{V_{turn}^2}{g\sqrt{n^2 - 1}}. \tag{11}$$

Such a new formulation allowed to split each lap into two different flight conditions: 1000 m cruise flight and a bank flight with a length of $2\pi T_R$ m. With that, relations for average airspeed, lift and drag coefficient were adopted:

$$V_{avg} = V_{cruise}(1 - \frac{2\pi T_R}{1000}) + V_{turn}\frac{2\pi T_R}{1000} \tag{12}$$

$$C_{L_{avg}} = C_{L_{cruise}}(1 - \frac{2\pi T_R}{1000}) + C_{L_{turn}}\frac{2\pi T_R}{1000} \tag{13}$$

$$C_{D_{avg}} = C_{D_{cruise}}(1 - \frac{2\pi T_R}{1000}) + C_{D_{turn}}\frac{2\pi T_R}{1000} \tag{14}$$

which in turn allow us to refine the range from Eq. (3) and endurance from Eq. (4):

$$R = \frac{m_{bat}}{m_{mav}g}B_{SE}\eta\frac{C_{L_{avg}}}{C_{D_{avg}}} \quad \text{and} \quad E = \frac{R}{V_{avg}} \tag{15}$$

5.2. *Aerodynamic calculation refinement*

In order to enhance the drag prediction in the MDO process, we used the wind tunnel test results at representative velocity to refine the drag calculation. As shown in Figure 16, motor arm drag can be assumed as constant at such speed for angles of attack lower than 15°. The payload+core drag was approximated with a second order polynomial function, varying according to the angle of attack. The wing drag, calculated with OpenAeroStruct, was kept without changes. The total drag was then calculated as:

$$C_D = C_{D_{OAS}} + C_{D_{core+payload}}(\alpha) + C_{D_{arms}} \tag{16}$$

For the lift, two changes were made: the predicted lift coefficient for alpha zero (C_{L0}) was updated from 0.2 (first MDO iteration) to zero, and a correction of 0.7 was also applied to the output of the OpenAeroStruct. These changes were made with the objective of fitting the predicted lift with the experimental result.

5.3. *Weight module refinement*

The weight prediction of the components was also updated considering the information gathered with the first vehicle, as shown in Table 8.

Table 8: Fixed weight refined breakdown.

Component	Mass
Motors and arms	104 $[g]$
Cables	20 $[g]$
Wing density of area	1360 $[g/m^2]$

5.4. *Refined MDO formulation and optimized vehicle*

The XDSM presented in Figure 21 and Table 9 show the new configuration of the MDO problem, with the added design variable and constraints. In order to comply with manufacturing technique limitations, as problems occurred when printing larger wing spans and smaller tip chords, the bound constraints were changed, reducing the design space.

As the wind tunnel and flight test campaigns were fully conducted considering the initially defined payload of 0.2 kg, this value was fixed in order to ensure precise drag prediction and avoid extrapolations with untested payloads. Even if the score analysis previously presented could have been refined considering the new data, we considered that the trends observed with the first MDO problem were still valid.

Table 9: MDO problem formulation with new design variable and constraints highlighted.

	Function/Variable	Lower	Upper
Maximize	Score		
With respect to	Root chord	0.125 m	0.2 m
	Tip chord	0.095 m	0.2 m
	Span	0.3 m	0.7 m
	Cruise α	1°	10°
	Turn α	1°	8°
	Battery mass	0.1 kg	0.2 kg
Subject to	Endurance $\leq$ 23 min		
	$\mathbf{a_{hover}} \geq 0$		
	$\mathbf{a_{turn}} \geq 0$		

For this execution we used the super efficient global optimization coupled with mixture of experts (SEGOMOE),[26] a surrogate-based gradient-free optimizer that can handle expensive and multimodal cases, in order to avoid converging to a local optima. Table 10 shows the characteristics of the second iteration of the vehicle.

Table 10: Optimal MAV characteristics at the end of new MDO iteration.

Design variables	Value
Root chord	0.12 m
Tip chord	0.095 m
Wing span	0.7 m
Cruise α	10°
Turn α	8°
Battery mass	0.2 kg
Coupling variables	**Value**
Wing area	0.075 m^2
Cruise speed	18.0 m/s
Cruise C_L	0.54
Cruise C_D	0.12
Flight time	14.6min
Number of laps	13
MAV mass	0.74 kg

6. Competition and endurance test results

Throughout the design iterations and test flights, 4-cell LiPo battery with 1800 mAh was employed. However, before the competition a better option was found with the same mass of 200 g, which had a specific energy of 177 $\frac{Wh}{kg}$, that is 44 $\frac{Wh}{kg}$ more than the original battery. With the new battery, the flight time was expected to increase approximately 30% more than the MDO process prediction. Figure 22 shows the ready to fly version of the vehicle for IMAV2022 competition with a total weight of 720 g including the 200 g payload.

Fig. 22: Vehicle ready for competition.

The total time in the competition slot was 30 minutes. During more than half of this time, the vehicle presented a problem with the autonomous guidance and navigation module, which is out of the scope of this paper. However, this problem was solved on time and the vehicle flew fully autonomously for the remaining 13 minutes, completing 7 laps, as shown in Figure 23. This competition flight consumed roughly 1770 mAh, 73% of the battery nominal energy.

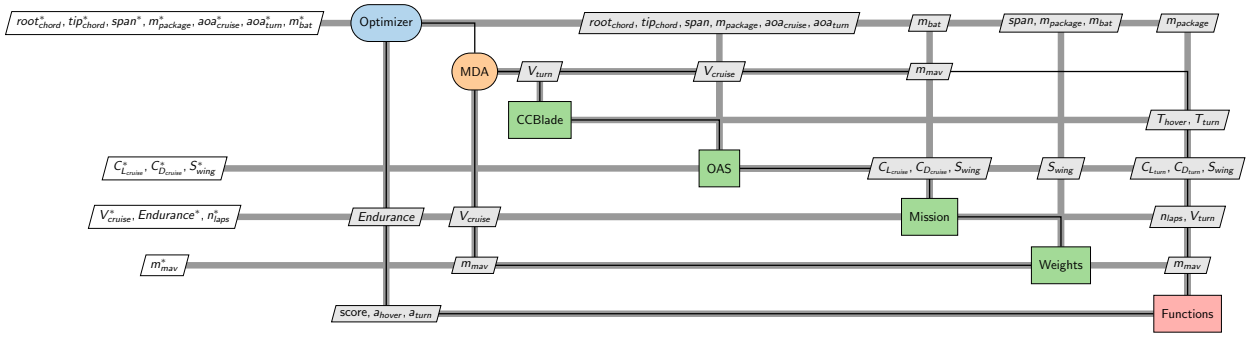

Fig. 21: Extended design structure matrix of the refined tail-sitter process.

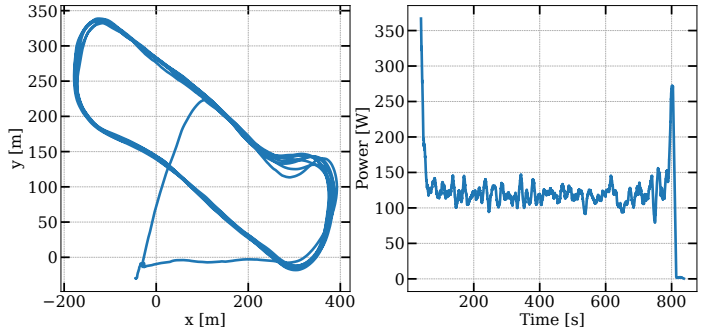

Fig. 23: Flight trajectory and power consumption in the competition run.

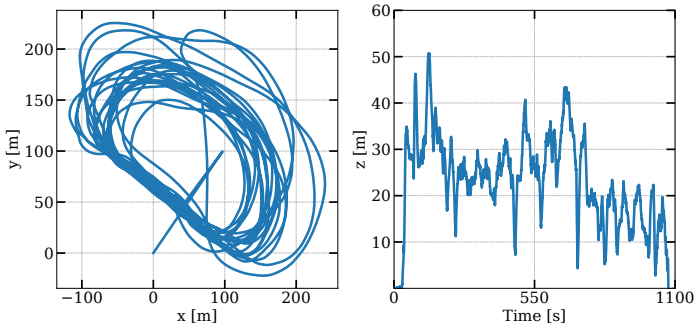

Fig. 24: Flight trajectory in the endurance test.

This flight was sufficient to ensure the first place in the competition, along the other vehicles from the same team performing different missions, but not enough to conclude about the total endurance performance. Therefore, after the competition, we scheduled a new test flight test to measure the endurance performance of the design. Such endurance test was performed in Muret, close to Toulouse, two weeks after the IMAV2022 conference. The wind speed was reaching up to 10 m/s during the test day, which caused a change in the flight plan. After the takeoff, the guidance system misbehaved while trying to turn with crosswind. In order to handle that and secure the desired endurance information, we changed to direct mode, using only the attitude control loop from the autopilot. Such change impacted the flight trajectory, which is not as precise as the others, as it can be seen in Figure 24. However, it did not impact the quality of the observed data and the test turned out to be an approximately 18-minute long successful flight.

It is possible to observe that the power consumption, shown in Figure 25, is substantially smaller than the one shown in Figure 9, which justifies the difference in flight time between the design iterations.

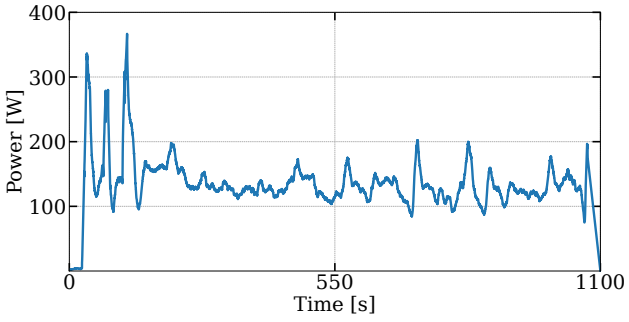

Fig. 25: Power consumption in the endurance test.

As discussed, such difference can be mainly attributed to the pitch angle. Figure 26 shows the pitch angle in the endurance test. Even if in such a windy day it is more difficult to estimate the angle of attack by observing the pitch angle, it is possible to observe that the values were considerably smaller than the ones shown in Figure 19.

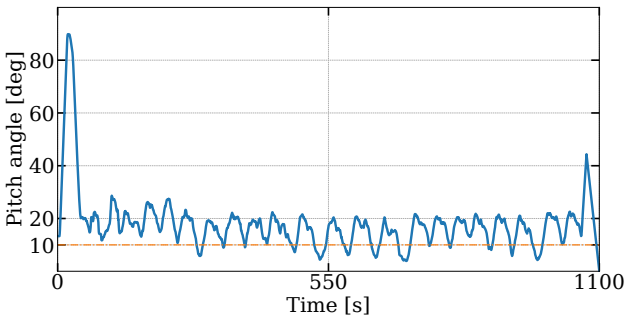

Fig. 26: Pitch angle in the endurance test.

7. Conclusion

We presented a full design and flight testing cycle of a Tail-sitter MAV. The vehicle was designed to comply with the IMAV 2022 competition rules, which offers an interesting benchmark for evaluating a design methodology. A multidisciplinary design and optimization approach was selected. The first MDO was a combination of three disciplines: aerodynamics, weights, and mission analysis, and it led to a smaller design, which was built and flight tested. Wind tunnel tests are conducted to refine both lift and drag prediction, and CCBlade is employed for thrust analysis in both hover and turn maneuver conditions, leading to reduced energy consumption. The design obtained after the second iteration of the MDO presented a more accurate lift prediction, in line with the expectations, which in turn resulted in lower energy consumption during preliminary test flights. The presented MDO methodology can be applied for different missions by adapting the bounds for the design variables and changing the objective function and constraints formulation as required. In the IMAV2022 "Package delivery challenge", despite having problems with guidance and autonomous navigation modules, the vehicle flew for around 13 minutes, winning the first place. After the competition, an 18-minutes long endurance was reached during a flight test. There are two different lines to be addressed in future work. In order to allow for more design freedom, with for instance bigger wing spans and variable wing twist, we will refine the manufacturing process. To make the design methodology more reliable, the simulation of the closed loop vehicle dynamics will be added as a different discipline.

Acknowledgments

This work is part of the activities of ONERA - ISAE - ENAC joint research group. The authors also thank the other members of ENAC team for the IMAV22 competition, who helped throughout the preparation of the Falcon and other drones: Gautier Hattenberger, Xavier Paris, Fabien Bonneval, Florian Sansou, and Zeynep Bilgin.

References

[1] E. Ausonio, P. Bagnerini and M. Ghio, Drone swarms in fire suppression activities: A conceptual framework, *Drones* **5**(1) (2021).

[2] M. A. Akhloufi, A. Couturier and N. A. Castro, Unmanned aerial vehicles for wildland fires: Sensing, perception, cooperation and assistance, *Drones* **5**(1) (2021).

[3] Y. Taddia, C. Corbau, J. Buoninsegni, U. Simeoni and A. Pellegrinelli, Uav approach for detecting plastic marine debris on the beach: A case study in the po river delta (italy), *Drones* **5**(4) (2021).

[4] A. Restás, Drone applications fighting covid-19 pandemic;towards good practices, *Drones* **6**(1) (2022).

[5] Z. Zhang and D. Scaramuzza, Perception-aware receding horizon navigation for mavs, *2018 IEEE International Conference on Robotics and Automation (ICRA)*, (IEEE Press, 2018), p. 2534–2541.

[6] K. Y. Scheper and G. C. de Croon, Evolution of robust high speed optical-flow-based landing for autonomous mavs, *Robotics and Autonomous Systems* **124** (2020) p. 103380.

[7] R. Ritz and R. D'Andrea, A global controller for flying wing tailsitter vehicles, *2017 IEEE International Conference on Robotics and Automation (ICRA)*, (2017), pp. 2731–2738.

[8] P. Hartmann, C. Meyer and D. Moormann, Unified velocity control and flight state transition of unmanned tilt-wing aircraft, *Journal of Guidance, Control, and Dynamics* **40**(6) (2017) 1348–1359.

[9] E. J. J. Smeur, M. Bronz and G. C. H. E. de Croon, Incremental control and guidance of hybrid aircraft applied to a tailsitter unmanned air vehicle, *Journal of Guidance, Control, and Dynamics* **43**(2) (2020) 274–287.

[10] B. Wang, Z. Hou, Z. Liu, Q. Chen and X. Zhu, Preliminary design of a small unmanned battery powered tailsitter, *International Journal of Aerospace Engineering* **2016** (May 2016) p. 3570581.

[11] J. Holsten, T. Ostermann and D. Moormann, Design and wind tunnel tests of a tiltwing uav, *CEAS Aeronautical Journal* **2** (Dec 2011) 69–79.

[12] T. Vogeltanz, Conceptual design and control of twin-propeller tail-sitter mini-uav, *CEAS Aeronautical Journal* **10** (Sep 2019) 937–954.

[13] G. J. Ducard and M. Allenspach, Review of designs and flight control techniques of hybrid and convertible vtol uavs, *Aerospace Science and Technology* **118** (2021) p. 107035.

[14] A. B. Lambe and J. R. R. A. Martins, Extensions to the design structure matrix for the description of multidisciplinary design, analysis, and optimization processes, *Structural and Multidisciplinary Optimization* **46** (2012) 273–284.

[15] R. Lafage, S. Defoort and T. Lefebvre, Whatsopt: a web application for multidisciplinary design analysis and optimization, *AIAA Aviation 2019 Forum*, Dal-

las, Texas (June 2019).
[16] J. R. R. A. Martins and A. B. Lambe, Multidisciplinary design optimization: A survey of architectures, *AIAA Journal* **51** (September 2013) 2049–2075.
[17] J. P. Jasa, J. T. Hwang and J. R. R. A. Martins, Open-source coupled aerostructural optimization using Python, *Structural and Multidisciplinary Optimization* **57** (April 2018) 1815–1827.
[18] J. Carvill, 4 - fluid mechanics, *Mechanical Engineer's Data Handbook*, ed. J. Carvill (Butterworth-Heinemann, Oxford, 1993), pp. 146–171.
[19] M. Bronz, E. Tal, F. Favalli and S. Karaman, Mission-oriented additive manufacturing of modular mini-uavs, *AIAA Scitech 2020 Forum*, Orlando, FL (January 2020).
[20] J. S. Gray, J. T. Hwang, J. R. R. A. Martins, K. T. Moore and B. A. Naylor, OpenMDAO: An open-source framework for multidisciplinary design, analysis, and optimization, *Structural and Multidisciplinary Optimization* **59** (April 2019) 1075–1104.
[21] N. Wu, G. Kenway, C. A. Mader, J. Jasa and J. R. R. A. Martins, pyoptsparse: A python framework for large-scale constrained nonlinear optimization of sparse systems, *Journal of Open Source Software* **5**(54) (2020) p. 2564.
[22] P. Brisset, A. Drouin, M. Gorraz, P.-S. Huard and J. Tyler, The paparazzi solution, *IMAV 2006*, Braunschweig, Germany (October 2006).
[23] A. Ning, Using blade element momentum methods with gradient-based design optimization, *Structural and Multidisciplinary Optimization* **64** (August 2021) 991–1014.
[24] M. Drela, Xfoil: An analysis and design system for low reynolds number airfoils, *Low Reynolds Number Aerodynamics*, ed. T. J. Mueller (Springer Berlin Heidelberg, Berlin, Heidelberg, 1989), pp. 1–12.
[25] L. F. Fernandez, M. Bronz, N. Bartoli and T. Lefebvre, Assessment of methods for propeller performance calculation at high incidence angles, *AIAA SCITECH 2023 Forum*, National Harbour, US (January 2023).
[26] N. Bartoli, T. Lefebvre, S. Dubreuil, R. Olivanti, R. Priem, N. Bons, J. R. R. A. Martins and J. Morlier, Adaptive modeling strategy for constrained global optimization with application to aerodynamic wing design, *Aerospace Science and Technology* **90** (July 2019) 85–102.

Luiz F. Tiberio Fernandez is a PhD student at ONERA and ENAC. Before moving to France, he received his M.S in Aeronautical Engineering from the Aeronautics Institute of Technology (Brazil) studying aircraft design and MDO, and worked as a product development engineer for EMBRAER (Brazil) as a part of the team responsible for the flight control software of the second generation of E-Jets.

Murat Bronz received his master's degree from Istanbul Technical University on Aeronautical and Astronautical Engineering. Later, he received his PhD on "Long Endurance Mini-UAV Design" from ISAE in 2012. Since April 2013, he has been working as an Assistant Professor at ENAC. His research topics evolved during the years, starting from aircraft design towards control, guidance and intelligence. The ultimate objective is to improve the operational capabilities of small aerial vehicles by increasing their aerodynamic efficiency, flight performance, self-awareness, and collaborations. Experimentation and real-life performance of the mentioned concepts lies in the core of his works. He designed several micro air vehicles, some with solar-powered, unconventional configurations that had vertical take-off and landing capabilities (VTOL) and flight tested each one of them. Right now, he is discovering the potential of learning based methodologies for design, control and guidance of these vehicles applied to single and multi-agent missions.

Nathalie Bartoli received the Eng. Diploma and Ph.D. Degree in applied mathematics from the National Institute of Applied Sciences of Toulouse, France, in 1997 and 2000, respectively. From 2000 to 2005, she worked 5 years as a researcher in the Electromagnetism Team at CERFACS (European Center for Research and Advanced Training in Scientific Computation). Since 2005, she is doing research at ONERA in the applied mathematics domain. In 2012, she joined the MDO and conceptual aircraft design team at ONERA, where she has worked ever since as Senior Research Scientist In December 2019, she defended her academic accreditation to supervise research (HDR) in Applied Mathematics. Her research interests include surrogate models and multidisciplinary optimization (MDO). She worked on surrogate-based optimization techniques within the framework of national projects or Europeans, with a joint supervision of several PhDs on these subjects. She was involved in AGILE H2020 project (Aircraft 3rd Generation MDO for Innovative Collaboration of Heterogeneous Teams of Experts, 2015-2018) and she is currently involved in AGILE 4.0 (2019-2022). She is also Professor at ISAE-SUPAERO with some optimization and

MDO courses. Since 2017, she is a member of the AIAA MDO Technical Committee.

Thierry Lefebvre, graduated from Arts et Métiers Paris Tech in 2000 and from IFP School in 2002. He joined ONERA in 2002, as a research engineer in the Applied Aerodynamics Department (DAAP), working on the optimization of tilt-rotor blades within EU projects. In 2008, he moved to ONERA Toulouse to focus on advanced aircraft design methods, including Multidisciplinary Optimization and Surrogate models. He was involved in AGILE H2020 project (Aircraft 3rd Generation MDO for Innovative Collaboration of Heterogeneous Teams of Experts, 2015-2018) and in the follow-up project AGILE 4.0 (2019-2022). His works concentrate on multidisciplinary design and optimization of systems applied to future aircraft.